Advances in Science and Technology Research Journal

Advances in Science and Technology Research Journal 2023, 17(6), 228–244
https://doi.org/10.12913/22998624/174109
ISSN 2299-8624, License CC-BY 4.0

Received: 2023.09.25
Accepted: 2023.10.13
Published: 2023.11.21

Numerical and Experimental Studies on 3D Printed Compliant Mechanisms in Gripper Applications

Piotr Wiesław Niedziałek[1], Aleksy Figurski[1], Michał Piotr Kowalik[1*]

[1] Institute of Aeronautics and Applied Mechanics (IAAM), Warsaw University of Technology, Plac Politechniki 1, 00-661 Warszawa, Poland

* Corresponding author's e-mail: michal.kowalik@pw.edu.pl

ABSTRACT

The article describes two versions of a gripper's fingers that utilize compliant revolute kinematic pairs in their operation. The goal in designing the gripper was to create a universal structure that allows for easy adjustment of torsional stiffness and maximum rotation angle as needed. Two compliant revolute joints were proposed and applied in the creation of two versions of the gripper's fingers. In both joints, one geometric parameter was selected for variation. Finite element analysis was conducted to calculate the statics within the parameter range. Based on the calculations, stiffness charts were created as a function of parameter values. Subsequently, using 3D printing technology in resin, two gripper fingers were produced. Experimental tests were conducted on these fingers to assess their torsional stiffness. The computational and experimental results were compared. The designed fingers are best suited for pneumatic grippers. When using them, complex force control can be eliminated because the gripping force increases gradually in accordance with the compliance of the gripper, rather than abruptly. The fingers also exhibit different stiffness characteristics depending on the direction of the grip-outward or inward.

Keywords: compliant mechanism, compliant joint, compliant gripper.

INTRODUCTION

Compliant mechanisms are mechanisms in which the deformation of their components is utilized to achieve desired motion and transmit force and energy [1]. These mechanisms reduce the use of moving connections that require elements such as bearings, pins, screws, and hinges. As a result, a complex mechanism can often be replaced by a compliant mechanism consisting of only one part [2]. Compliant mechanisms are definitely simpler and often much cheaper to produce than their classical equivalents. They can be manufactured using methods such as 3D printing [3], injection molding, machining, laser cutting [4], and waterjet cutting. Compliant mechanisms are typically designed using finite element analysis, topology optimization [5], and the pseudo-rigid-body method [6].

Compliant mechanisms have found their application in kinematic pairs [7]. Such compliant joints are characterized by simple construction, minimal friction, and predictable performance. However, their greatest challenge is limited range of motion. Due to their numerous advantages, compliant kinematic pairs have been applied in robotics and are increasingly used in prosthetics [8, 9].

A challenge in designing kinematic pairs is conducting the appropriate strength calculations. Compliant mechanisms are characterized by nonlinear elasticity [10].

In robotics, compliant mechanisms are also used in gripper design [11, 12]. The most common solution is fingers for grippers that adapt their shape to the lifted object [13]. This improves the stress distribution on the lifted element and is a good solution for lifting delicate and fragile objects [14].

The aim of this work was to create universal fingers for a gripper using a compliant revolute kinematic pair. The goal was to apply a kinematic pair for which, by changing one geometric

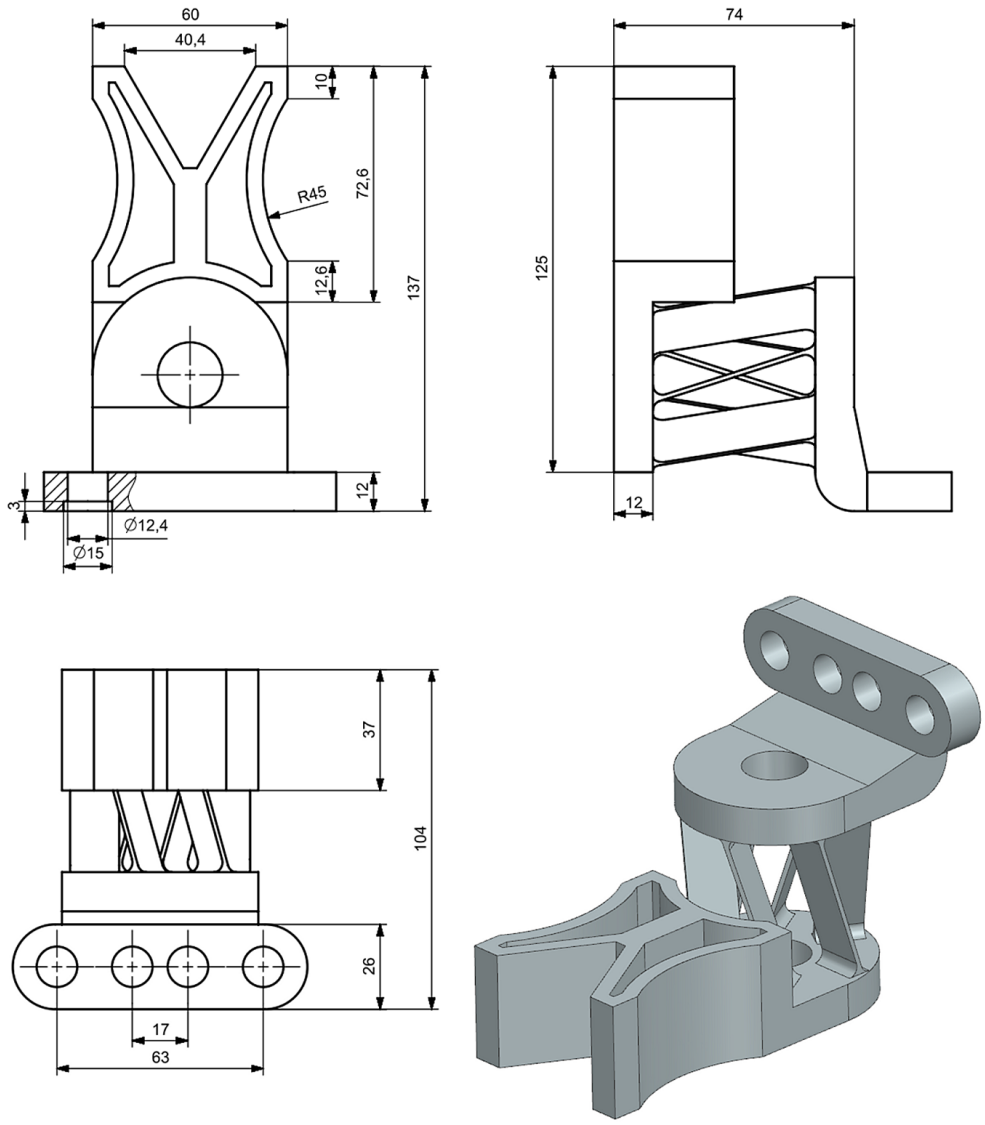

Fig. 1. The designed angled beams finger

parameter during modeling, the stiffness characteristics and maximum rotation angle can be altered in almost any way.

Two versions of fingers with two similar compliant revolute kinematic pairs were proposed. They differ only in the shape of the supports, as shown in Figures 1 and 2. The first one was named the "angled beams finger", and the second one the "twisted beams finger". Figure 3 illustrates the assembly of the fingers for a pneumatic gripper. The fingers can be installed in two configurations - for larger or smaller lifted objects. They can also be swapped sides.

The applied revolute kinematic pairs were parametrized. One characteristic dimension was selected for each. For successive parameter values, finite element method simulations were conducted. The calculations aimed to investigate torsional stiffness and range of rotation angles.

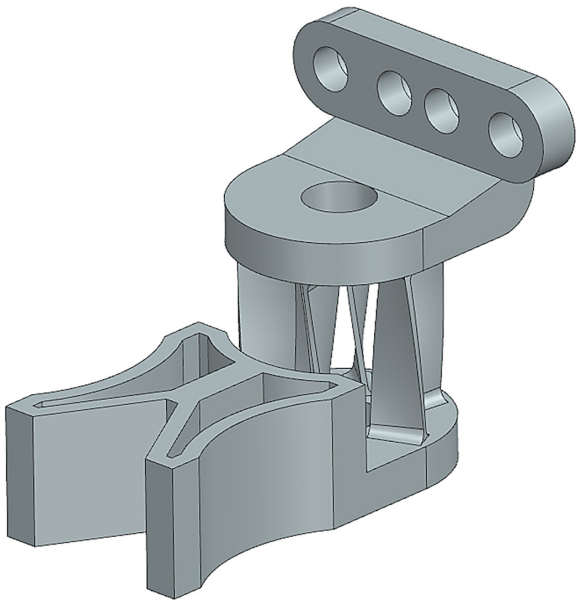

Fig. 2. The designed twisted beams finger

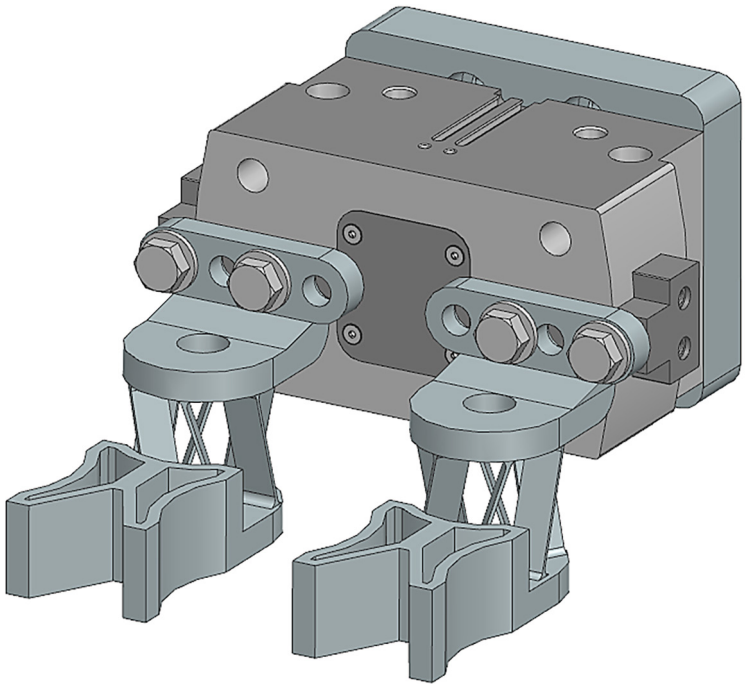

Fig. 3. Fingers mounted to a pneumatic gripper

Prototypes of the fingers were 3D printed in resin with the use of stereolithography due to lack of anisotropy which is problem in fused deposition modeling technology [15]. Experimental studies were conducted using them. A test stand as shown in Figure 4 was employed. The fingers were immobilized using a vice. A load was attached to the gripping end. The load was then varied in the range from 0.2 kg to 1 kg at intervals of 0.2 kg. A camera on a tripod took pictures of the fingers after each load change. The images were analyzed in a graphic program, and the rotation angles of the fingers relative to their initial positions were superimposed on them. The fingers were also loaded in the opposite direction.

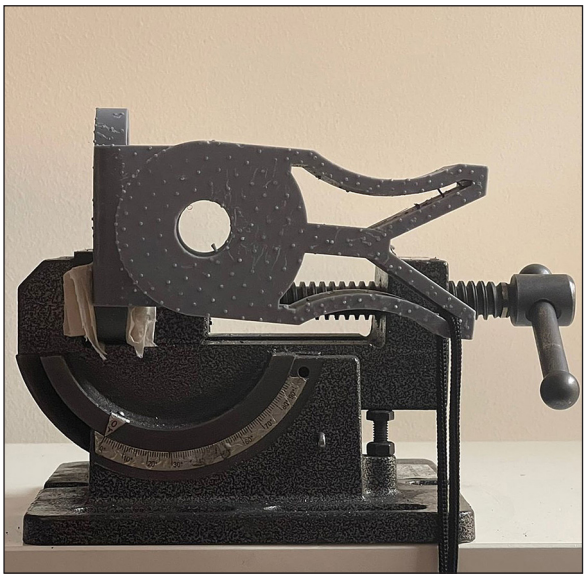

Fig. 4. Test stand

MATERIALS AND METHODS

Revolute kinematic pairs

The first stage of the work involved creating models of revolute kinematic pairs in the NX Siemens software. These models are similar to each other, differing only in the shape of the "supports" or their placement between the lower and upper bases. They are presented in the following Figures 5 and 6. The revolute kinematic pairs created by them operate as follows: the lower base is attached to one part, around which the second part rotates. The second part is attached to the upper base. The movement consists of rotating one base relative to the other. Rotation can only occur about one axis passing through the center of both bases. These pairs should be rigid in all other directions of rotation and displacement. Names were introduced: kinematic pair with angled beams and kinematic pair with twisted beams.

The next step was parameterization. One parameter was selected for each pair, in such a way as not to disturb the general geometry of the pairs but only to change the shape of the supports.

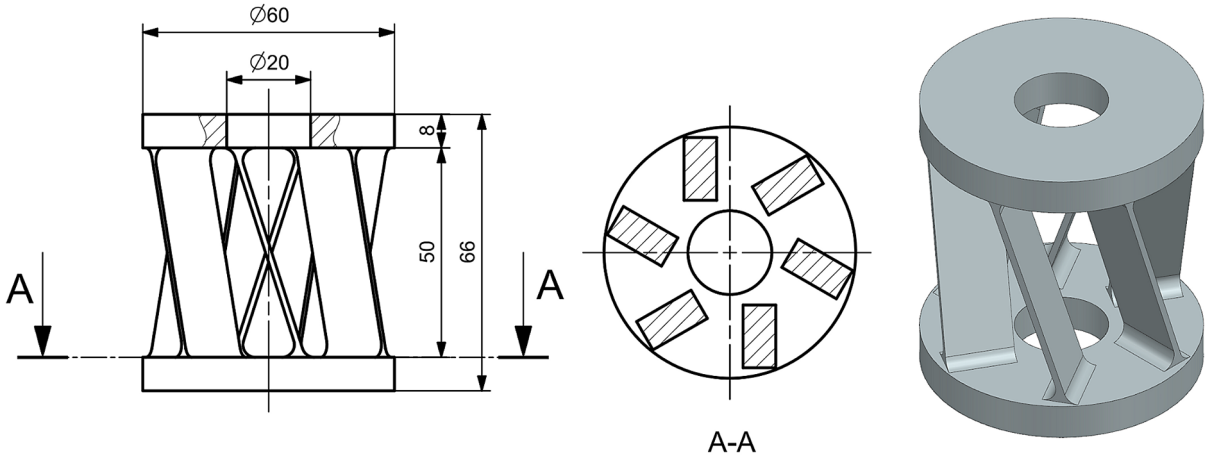

Fig. 5. Kinematic pair with angled beams

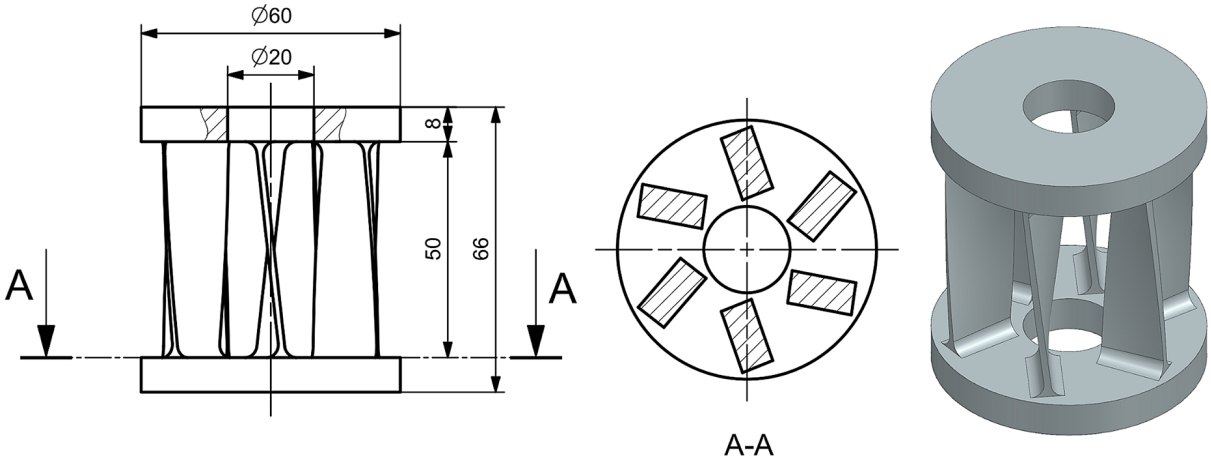

Fig. 6. Kinematic pair with twisted beams

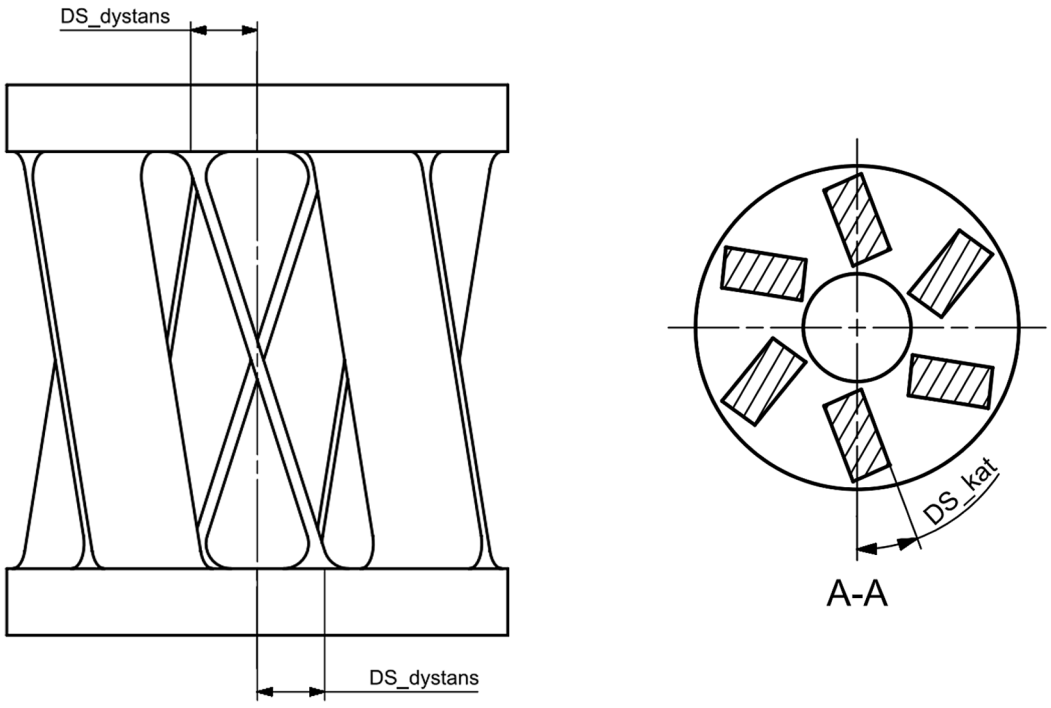

Fig. 7. Parametrized dimensions

For the model with angled beams, the decision was made to change the angle of inclination of the supports relative to the bases. This was implemented as shown in Figure 7. The bases of the supports were symmetrically moved from the model's axis. For the model with twisted beams, the angle shown in Figure 7 was parameterized. This angle is also present on the opposite base. Changing this parameter causes the 'twisting' of the supports. All beams belonging to one of the models have the same geometry.

Ranges of variation were selected for both parameters. The parameter "DS_distance" was varied from 0 to 8 mm. Above this value, the beams protruded beyond the base. This can be converted into tilt angle values from 72.25° to 90°. The limits of the parameter "DS_kat" are from 0° to 45°. Above this value, the twist of the beams caused problems in calculations.

Finite element method

Static calculations were conducted on the models using Ansys Mechanical software. Resin material was assigned to the models and manually added to the Ansys library. The properties of the resin used for 3D printing were utilized. The data about resin was obtained from the manufacturer's website [16]. A linear material model was assumed. The data is presented in Table 1.

Table 1. Mechanical and physical properties

Density	1100 kg/m^3
Young's Modulus	1037 MPa
Poisson's ratio	0.37
Ultimate tensile strength	24 MPa

For both models, the same global mesh settings were applied. In the mesh settings, the element size was changed to 2 mm. Additionally, the physics preference was changed to 'nonlinear mechanical.' This is a recommended setting for nonlinear solutions and brings several changes compared to the default 'mechanical' setting. The most significant difference is the more restrictive mesh checking, resulting in a mesh with a larger number of elements. Compliant mechanisms exhibit structural nonlinearity, hence the necessity of using such settings. Meshing for the two models was implemented in different ways.

The model with angled beams was divided into parts: two bases and six beams. This facilitated mesh generation. The 'sweep' method was selected. For this method, the mesher identifies surfaces of the model that are opposite each other. Subsequently, a 2D mesh is generated on one of the surfaces and copied to the other surface. Additional layers of elements are then added between the surfaces, following the model's topology. The advantage of this mesh generation method is a shorter generation time and a regular mesh structure. This method was chosen for all parts of the model.

Several changes were made in its settings. The element type was set to 'quadratic.' This results in the generation of a greater number of nodes within the elements than in the 'linear' setting, as an additional node is added along the lateral edge of the element. This setting is advantageous for better mesh fitting to the geometry. Another changed setting was the 'free mesh type.' This function determines the type of elements used to fill the volume. Hexahedral elements were chosen. The number of mesh divisions, i.e., the number of layers of elements added, was set to '4' for the bases and '10' for the beams.

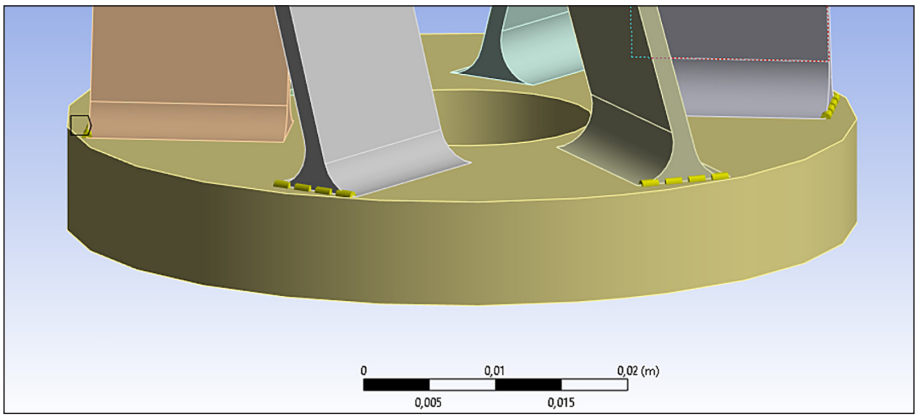

Fig. 8. Highlighted edges of the model with angled beams

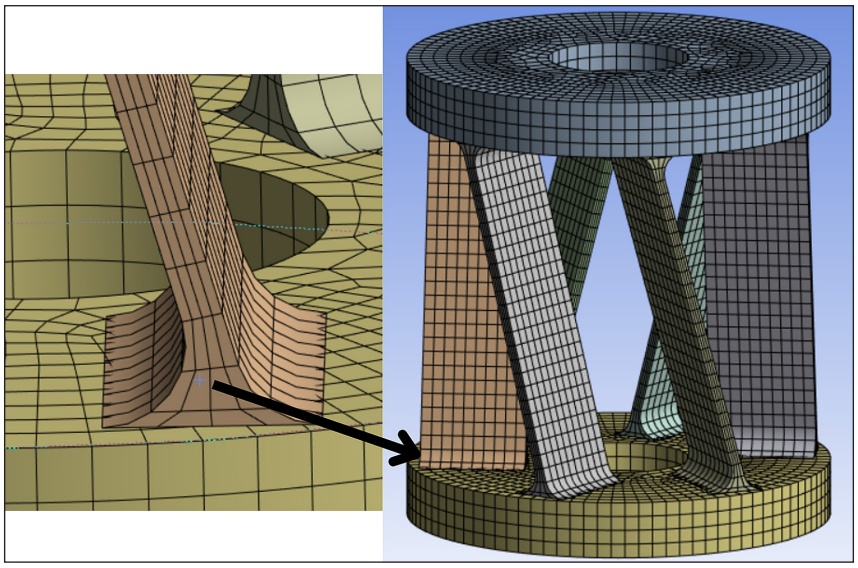

Fig. 9. Mesh of the model with angled beams

Table 2. Detailed mesh information - model with angled beams

Nodes	Elements	Element type	Element order
69406	13560	15 node wedge – 8 20 noded hexahedron - 13552	quadratic

Using the 'edge sizing' tool, the division of the edges of the beams shown in Figure 8 was set. The edges of the beams at the upper base, not visible in the figure, were also divided. This division enforces a specified number of elements forming a given edge of the model. The number of divisions was set to '4.' The generated mesh is shown in Figure 9. Detailed information about the mesh is provided in the Table 2.

To generate the mesh for the model with twisted beams, a different approach was employed due to its more complex geometry. Using the 'sweep' method for mesh generation was unsuccessful, so the 'multizone' method was chosen. This method works in a similar way. The mesher automatically divides the model into parts where the 'sweep' method can be applied and parts that need to be filled with an irregular mesh.

In the method settings, the element type was changed to 'quadratic'. Using the 'edge sizing' tool, three groups of edges were selected. The first group was chosen similarly to the previous model. The second and third groups are shown in Figure 10. They were divided into '10' and '22' parts, respectively. The generated mesh is presented in Figure 11. Specific details regarding the mesh can be found in the Table 3.

The same boundary conditions were applied to both models. In Figure 12, the surface where

Table 3. Detailed mesh information - model with twisted beams

Nodes	Elements	Element type	Element order
72140	14400	20 noded hexahedron	quadratic

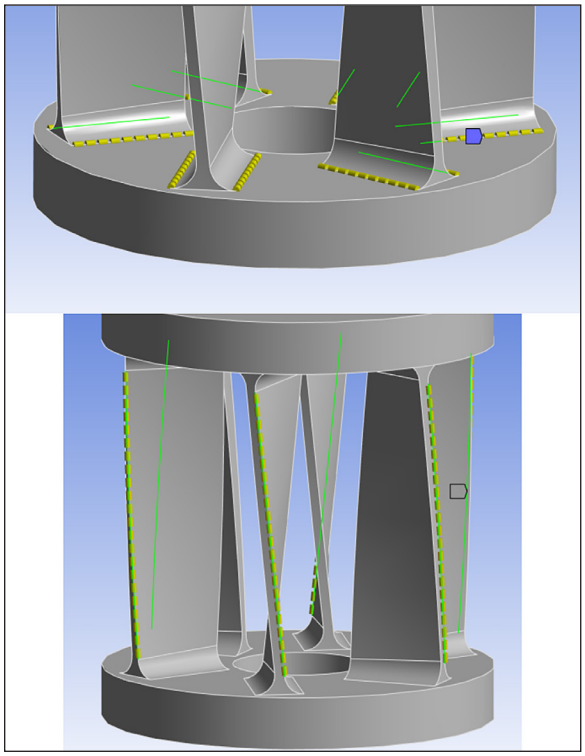

Fig. 10. Highlighted edges of the model with twisted beams

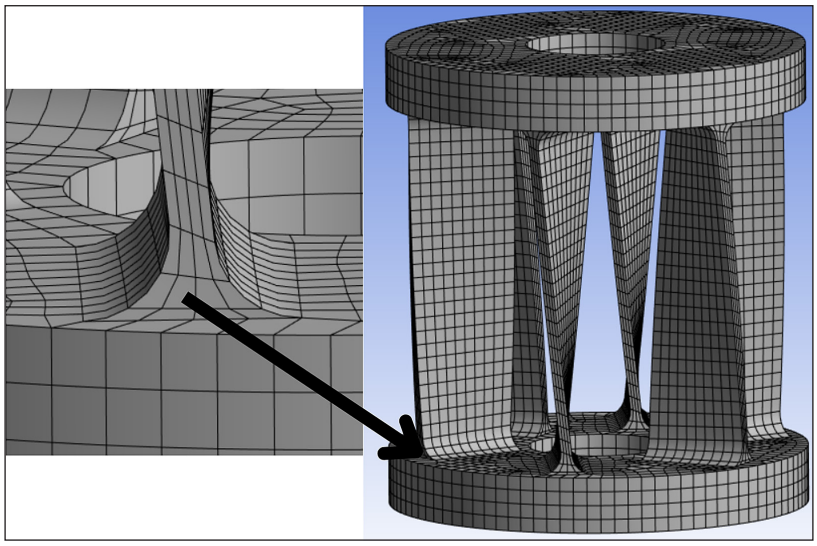

Fig. 11. Mesh of the model with twisted beams

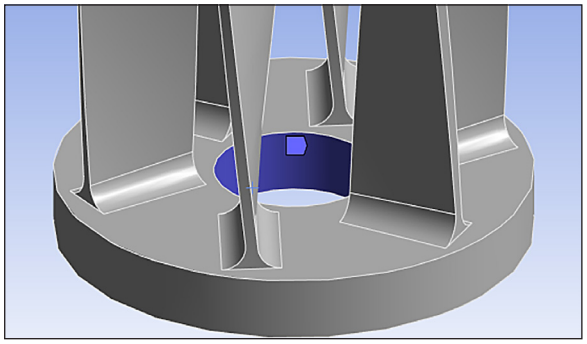

Fig. 12. Fixed support

all degrees of freedom were constrained using 'fixed support' is shown. This surface is located on the lower base of the model.

A torque was applied to the upper base surface. The moment vector is normal to the upper surface of the model, with its direction oriented upwards. This means that the joint is twisted counterclockwise around the axis passing through the centers of both bases. The moment was divided into ten steps from 0.1 Nm to 1 Nm. The location

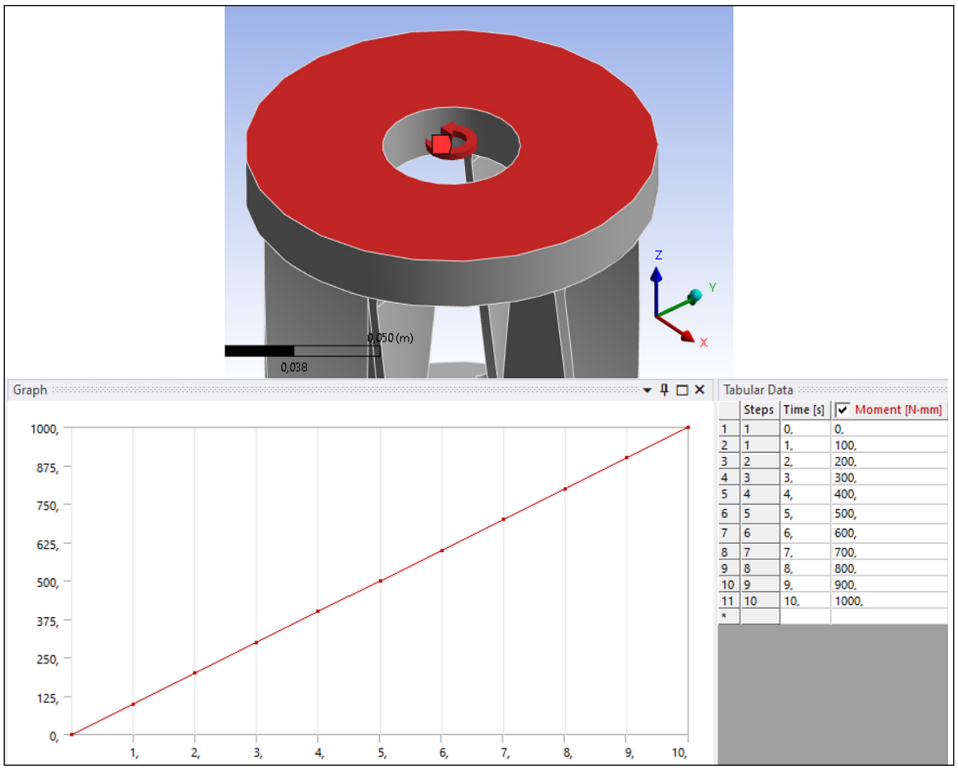

Fig. 13. Applied moment

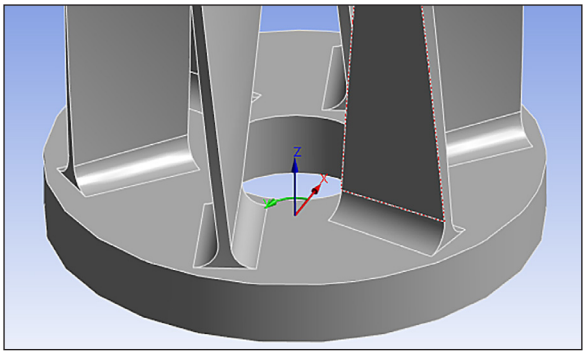

Fig. 14. Cylindrical coordinate system

of moment application and the moment curve are shown in Figure 13. Calculations were also performed for a moment acting clockwise.

An additional cylindrical coordinate system was added to better represent the results. The origin of the coordinate system is at the center of the hole on the plane of the lower base and is shown in Figure 14.

In the static analysis settings, the number of steps was set to '10.' This allowed the moment to be divided into steps and facilitated the solver in achieving convergence.

An important step was to enable the 'large deformations' option. This setting takes into account the change in the stiffness matrix 'K' depending on the geometry's deformation. For each iteration of calculations, the 'K' matrix is recalculated.

Displacement was prescribed in the 'y' direction in the created cylindrical coordinate system. From the obtained displacement, the rotation angle of the upper base relative to the lower one can be easily calculated. The maximum displacement is achieved at the outer edge of the upper base. By substituting this value into the formula, the rotation angle value is obtained. Calculations were performed for successive parameter values.

$$\Delta\theta = \frac{\Delta Y}{R} \tag{1}$$

where: ΔY – maximum displacement in the 'y' direction;
R – base radius.

RESULTS

Numerical studies

Based on the calculations for successive parameter values, the calculated points were plotted on graphs. The characteristics were approximated with polynomials ranging from 2nd to 5th degree.

Model with angled beams

The first plot in Figure 15 illustrates the relationship between the rotation angle of the upper base relative to the lower one and the angle of inclination of the beams. The calculation results for the torques described in the legend of the chart are presented. Based on this chart, you can determine which parameter value allowed for achieving the largest range of motion.

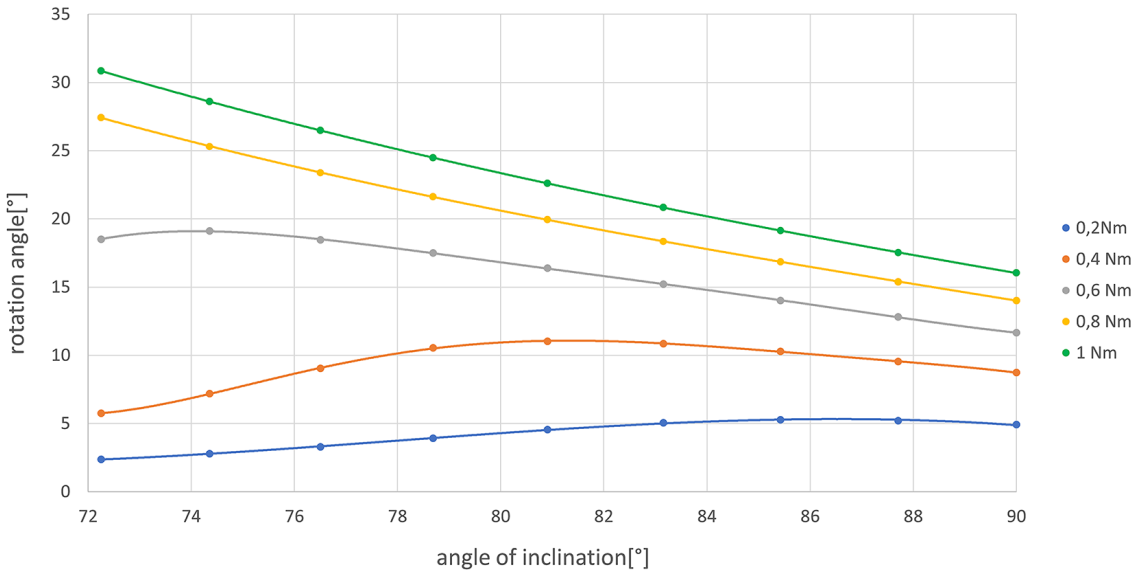

Fig. 15. Plot of the rotation angle against the angle of inclination for the model with angled beams

A slight change in the angle of inclination of the beams significantly affects the rotation angle. For the extreme points on the graph, the difference between the rotation angles is almost double - for 72.3°, a rotation angle of 30.84° was obtained, whereas for an inclination angle of 90°, this value was only 16.03°. For larger torques, i.e., 0.8 Nm and 1 Nm, the rotation angle decreases as the angle of inclination increases. However, for smaller moment values, the characteristics are not as regular. The rotation angle initially increases and then decreases. An interesting relationship is visible on the chart. The rotation angle is the largest for large moment values and the smallest for small moment values at the same angle of inclination. This phenomenon is more clearly visible in the subsequent charts and is explained further in the article.

The next plot in Figure 16 depicts the relationship between the rotation angle of the upper base relative to the lower one and the angle of inclination of the beams for a torque with the opposite direction.

The rotation angles for the moment with the opposite direction are significantly smaller. The shapes of the graphs are regular - the rotation

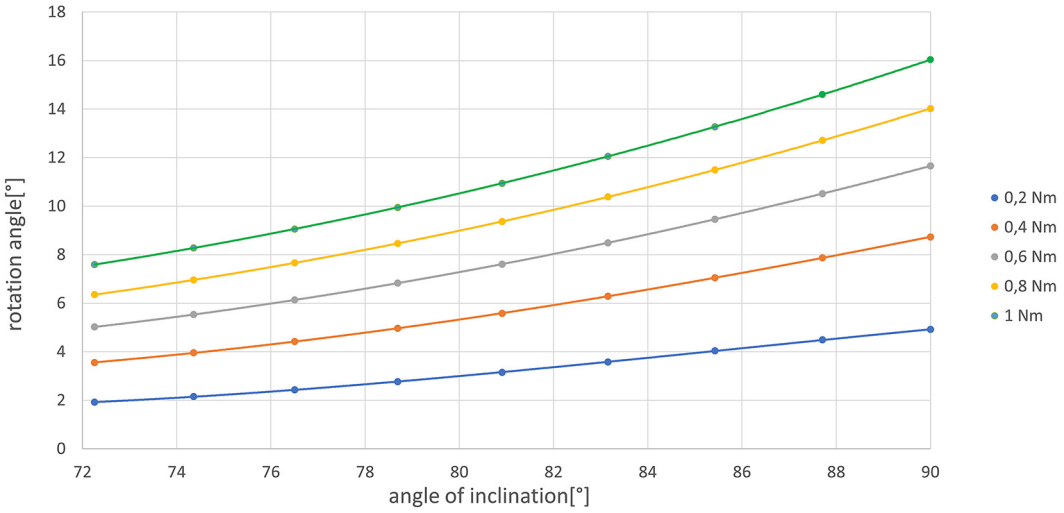

Fig. 16. Plot of the rotation angle against the angle of inclination for the model with angled beams – opposite direction of the moment

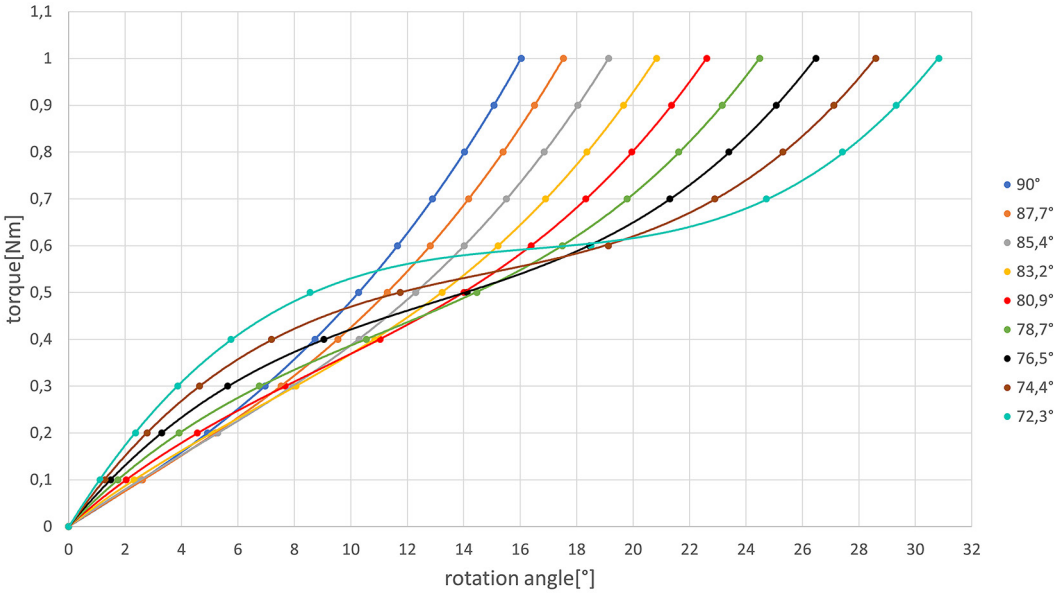

Fig. 17. Torsion characteristic of the model with angled beams

angle increases for successive points. For an angle of inclination of 90°, the rotation angle reaches its maximum and has the same value as in the previous chart - this is logical because for this case, the model's geometry is symmetrical. Small angles of beam inclination result in small rotation angles, which is the opposite of the previous chart.

The plot in Figure 17 illustrates the relationship between the torque and the rotation angle for the values of beam inclination shown in the legend. This is a torsion characteristic.

For values of the inclination angle parameter ranging from 80.9° to 90°, the stiffness of the models for a moment value of 0.2 Nm is very similar. At higher moment values, the stiffness starts to differ. For smaller angles of inclination, a similar lower stiffness is maintained up to higher moment values. For moment values above 0.7 Nm, the stiffness of these models becomes more similar - it is higher than at the beginning. Due to the longer segment of lower stiffness, models with smaller angles of inclination achieve greater rotation angles.

The characteristics of models with inclination angles from 72.3° to 78.7° have a similar shape. For small torque values, they exhibit higher stiffness, followed by a significant drop in stiffness at some point, before finally increasing again. Models with smaller beam inclination angles have higher initial stiffness on the graph but also a longer segment of lower stiffness, which results in the largest rotation angle among all the models. Characteristics for larger torques regain higher stiffness. Above 0.8 Nm, the stiffness of the models becomes similar. Models with larger angles of inclination are stiffer in this part.

For the model with an inclination angle of 72.3°, due to its most distinctive graph, the derivative was calculated. It is presented in Figure 18. Finite difference method was used to calculate the derivative. The derivative represents the torsional stiffness. The right y-axis corresponds to the derivative values.

Figure 19 shows the deformation of the model for successive values of the torque. Table 4 contains the rotation angles corresponding to the torques.

The derivative of the function is a second-degree polynomial. It reaches its minimum for a torque of approximately 0.6 Nm. The stiffness decreases to a value close to zero. Then it starts to increase, but it does not return to the same level

Table 4. Rotation angles of the model with angled beams for an inclination angle of 72.3°

Torque [Nm]	Rotation angle [°]
0.1	1.11
0.2	2.38
0.3	3.87
0.4	5.75
0.5	8.55
0.6	18.51
0.7	24.72
0.8	27.42
0.9	29.32
1	30.84

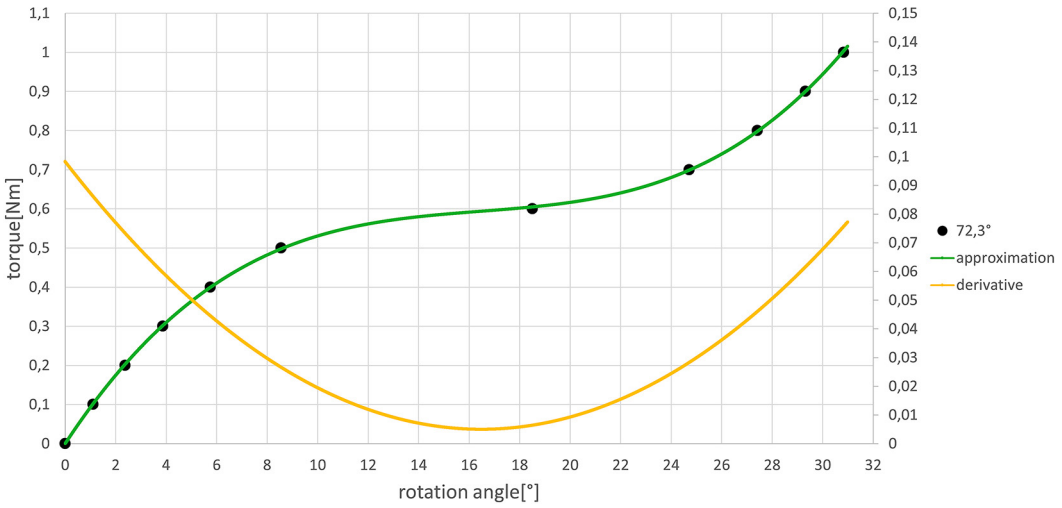

Fig. 18. Torsion characteristic of the model with angled beams for an inclination angle of 72.3°

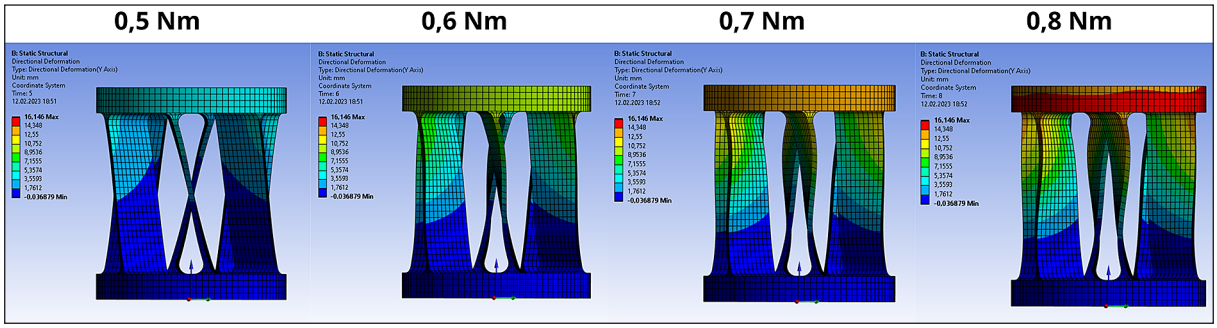

Fig. 19. Deformation of the model with angled beams for an inclination angle of 72.3°

as at the beginning. A torque of 0.5 Nm resulted in a small rotation angle of 8.55°. The beams between the bases slightly straightened, causing the upper base to rotate. The shape of the beams changed, and the beginning of the torsion is visible. Between the torque of 0.5 Nm and 0.6 Nm, there was a significant change in the rotation angle, increasing by approximately 10°. The beams are much more twisted, and their side walls take on a sinusoidal shape. Local instability occurred, leading to a significant decrease in stiffness. For a torque of 0.7 Nm, the beams are almost perpendicular to the base and undergo further torsion. The rotation angle continues to increase rapidly by about 6°. The beams experienced slight deformation between the torque of 0.7 Nm and 0.8 Nm, about 2.7°. Stability was regained. For subsequent torque values, the stiffness increases.

The stiffness was also examined for a torque in the opposite direction. The torsion characteristics for various values of beam inclination angles are shown in Figure 20.

In this case, the characteristics are regular. A smaller inclination angle of the beams results in greater stiffness across the entire characteristic range. For larger moment values, the models become stiffer.

Model with twisted beams

The graph in Figure 21 shows the angle of rotation as a function of the value of the "DS_kat" parameter. The characteristics in this graph were not approximated by a polynomial - this was not possible. The points are connected to each other using the chart type scatter with smoothed lines and markers in Excel.

Up to a certain parameter value, the angle of rotation increases and then decreases. The higher the torque value, the higher the parameter value for which the maximum occurs. For

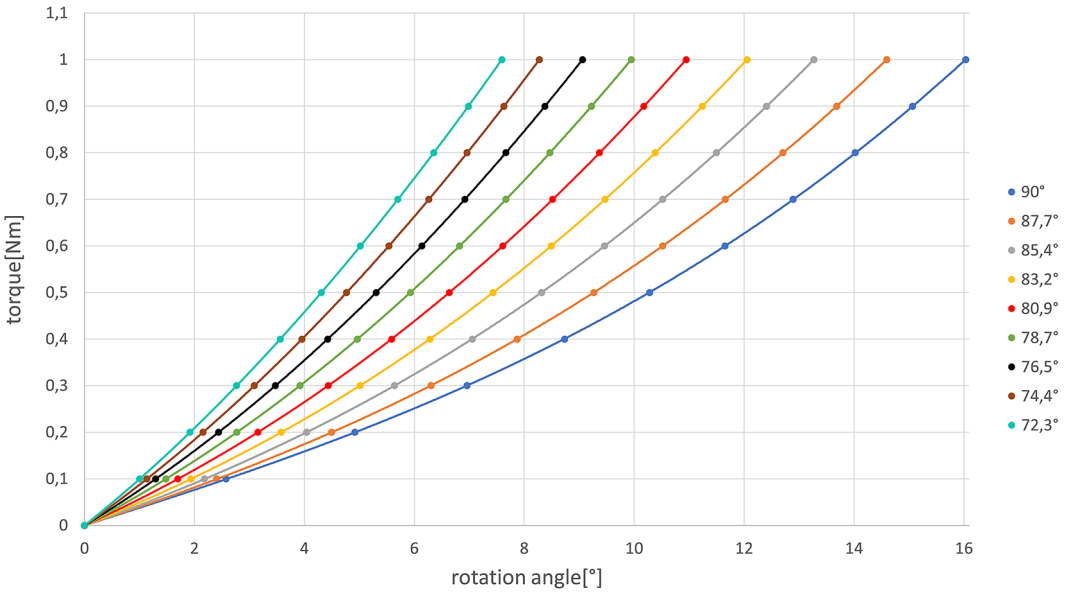

Fig. 20. Torsion characteristic of the model with angled beams – opposite direction of the moment

a torque of 0.8 Nm as well as 1 Nm, the largest rotation angle can be observed for a parameter value of about 25°.

The characteristics for the torque acting in the opposite direction are displayed in Figure 22. They exhibit regular patterns, with a similar trend for each torque value. The rotation angle decreases as the parameter value increases.

For the model with twisted beams, analogous diagrams were created. Figure 23 shows the torsion characteristic.

Characteristics for values of the parameter "DS_kat" from 0° to 10° follow a similar pattern. Up to a torque value of 0.2 Nm, they have very similar stiffness. As the torque increases, the stiffness of the models is lower for larger values of the parameter. The torsion characteristics for parameter values from 15° to 25° take an approximate form to the torsion characteristics of the angled beams models for small angles of inclination. The stiffness decreases significantly at one point and then increases to a similar level as before the drop. The initial stiffness increases as the value of the parameter increases.

The last group of characteristics is the group for parameter values above 30°. In this case, the

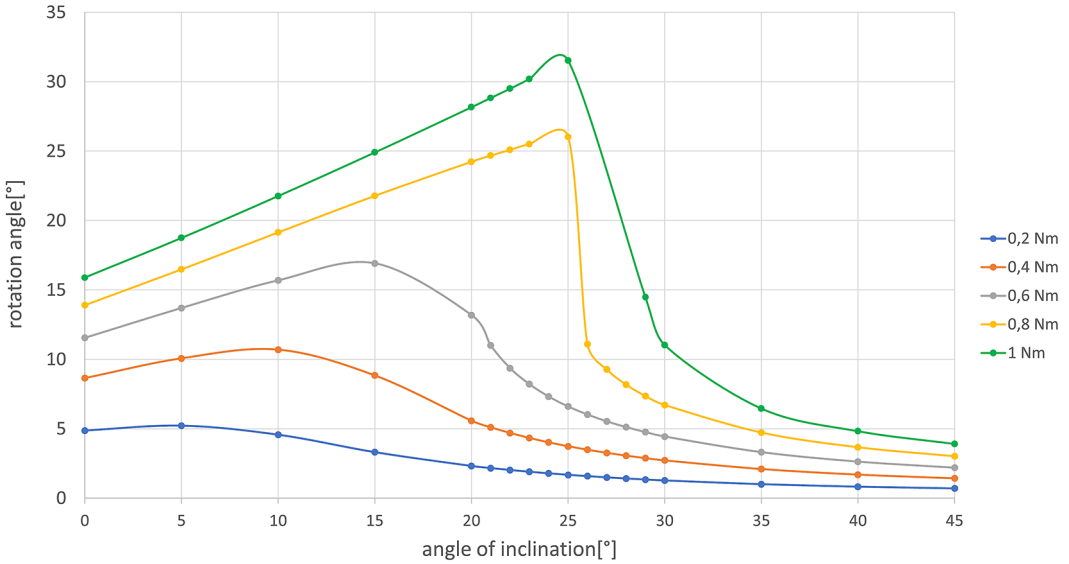

Fig. 21. Plot of the rotation angle against the angle of inclination for the model with twisted beams

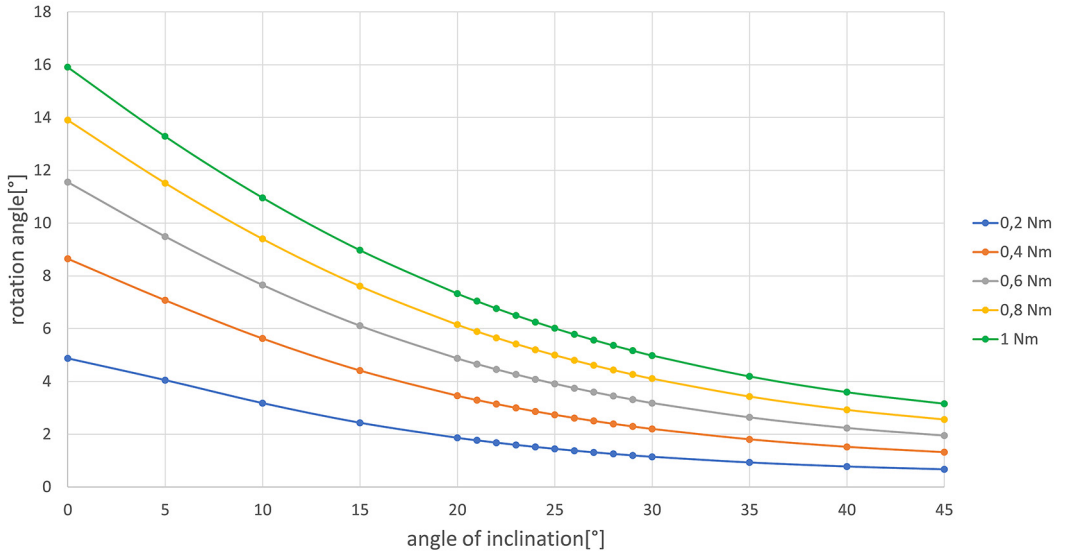

Fig. 22. Plot of the rotation angle against the angle of inclination for the model with twisted beams – opposite direction of the moment

stiffness is the highest. For 30 degrees, a collapse of the characteristic and a decrease in stiffness is visible. At the other values of the parameter, the stiffness changes little. Higher stiffness is found in models with a higher value of the parameter, "DS_kat".

Figure 24 shows the characteristic for the value of the parameter „DS_kat" 25°. The function was approximated by a third degree polynomial and its derivative was calculated. The model achieved the largest angle of rotation. The course of the characteristic is explained by showing the deformation of the model for successive values of the torque in Figure 25. Table 5 shows the angles of rotation and the corresponding moments.

Approximating the function with a third-degree polynomial proved to be less accurate in this case. It is impossible for the stiffness values to decrease below zero. However, the derivative accurately represents the nature of stiffness changes. In the case of this model, the initial stiffness is greater than that of the model with angled beams, and there is an even more significant decrease in stiffness.

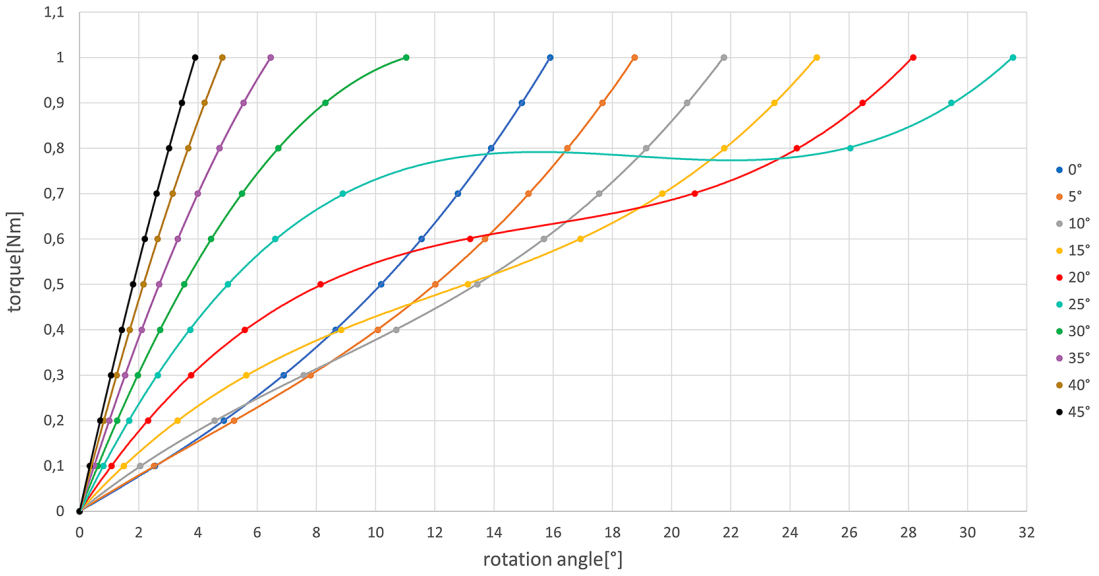

Fig. 23. Torsion characteristic of the model with twisted beams

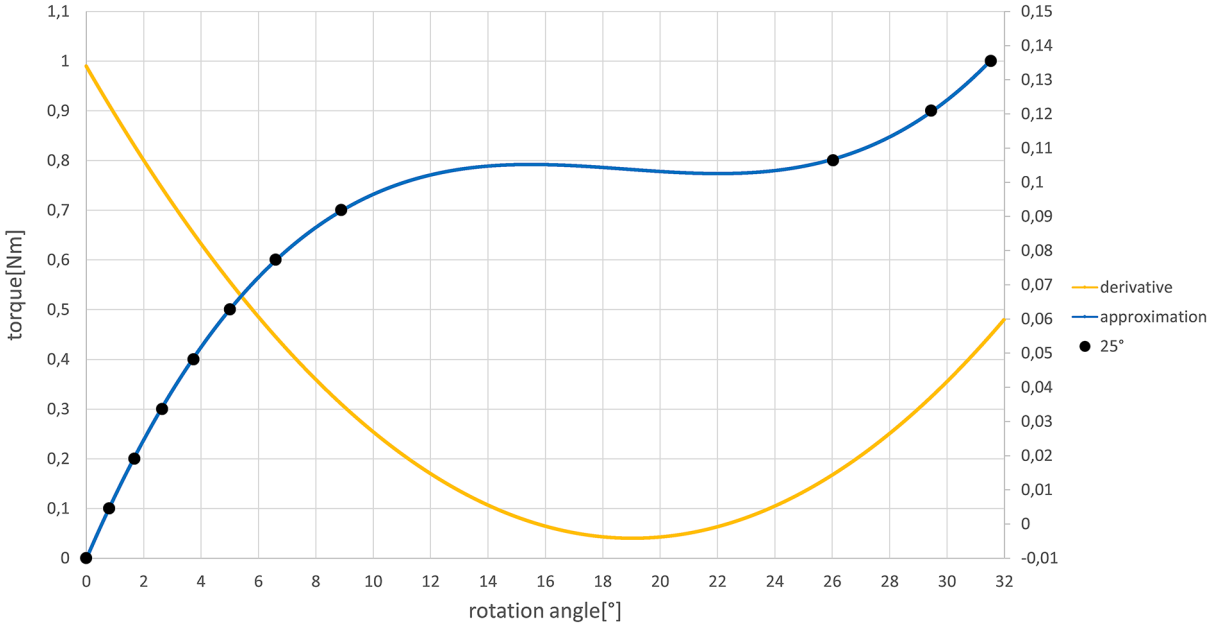

Fig. 24. Torsion characteristic of the model with twisted beams for the value of the parameter DS_kat 25°

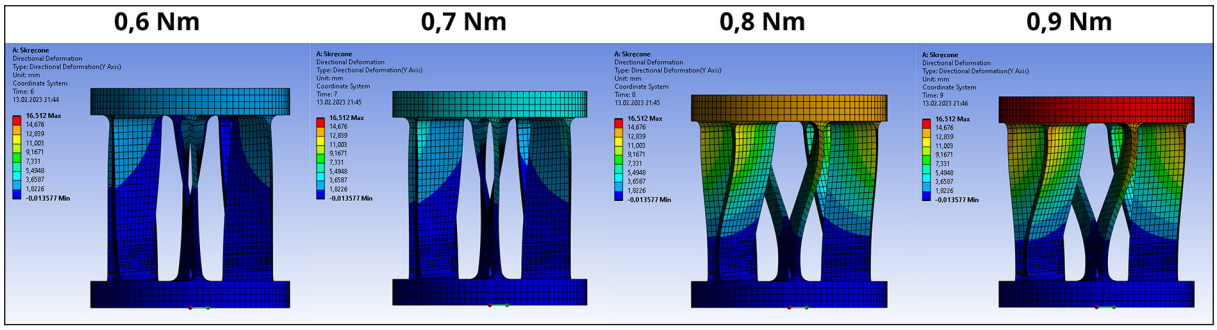

Fig. 25. Deformation of the model with twisted beams for the value of the parameter DS_kat 25°

Table 5. Rotation angles of the model with twisted beams for an inclination angle of 72.3°

Torque [Nm]	Rotation angle [°]
0.1	0.8
0.2	1.68
0.3	2.64
0.4	3.74
0.5	5.01
0.6	6.61
0.7	8.89
0.8	26.04
0.9	29.45
1	31.52

Ultimately, the rotation angle for a moment of 1 Nm was 31.52°, which is only 0.68° more than for the previously discussed model. Between moments of 0.6 Nm and 0.7 Nm, there is a slight change in the rotation angle, changing by 2.28°. The beams deform to a small extent. Then there is a very significant decrease in stiffness caused by local stability loss. The beams deflect visibly, and their side walls take on a sinusoidal shape. They are less twisted than initially. The rotation angle between moment values of 0.7 Nm and 0.8 Nm increases by as much as 17.15°. The change in angle for further moment increments is small, amounting to 3.41°. The beams tilt more and become less twisted, but their geometry changes to a much lesser extent.

The torsion characteristics for moments of opposite direction are visible in Figure 26. A smaller value of the parameter "DS_kat" signifies smaller stiffness across the entire range of the characteristic.

Experimental studies

Figure 27 illustrates the maximum obtained rotation angles for the finger with angled beams and the finger with twisted beams, respectively.

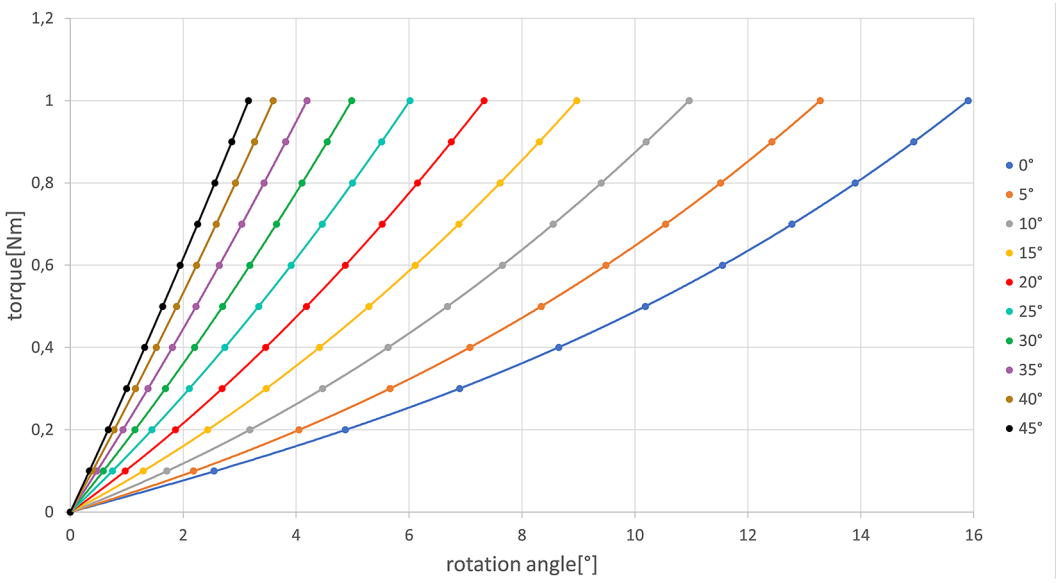

Fig. 26. Torsion characteristic of the model with twisted beams – opposite direction of the moment

The results are presented in Tables 6 and 7. Experimental results have been depicted in the graphs, with computed values also plotted. Polynomial approximations were applied to these graphs, as shown in Figures 28 and 29. The experiment was conducted on the finger with angled beams at an inclination angle of 72.3° and the finger with twisted beams with a "DS_kat" parameter value of 25°.

The experimentally determined rotation angle values differ from the calculations performed using the Finite Element Method. However, the overall shape of the graphs exhibits similar features. A similar stiffness reduction is observed in both experimental and computational results. In the case of moments of opposite direction, the profiles are even more closely aligned.

In the case of the model with twisted beams, experimental results also deviate from the calculations. However, the shape of the function is still similar. A challenge arises in the computational results due to polynomial approximation – in reality, stiffness cannot drop below zero, a fact supported by experimental results. For moments of opposite direction, the computational results diverge slightly more from the experimental ones.

Differences between numerical and experimental studies may also result from imperfections in the proposed method for experimentally verifying the results. Calculations were conducted only for the applied torsional moment, whereas in the experiment, bending moments

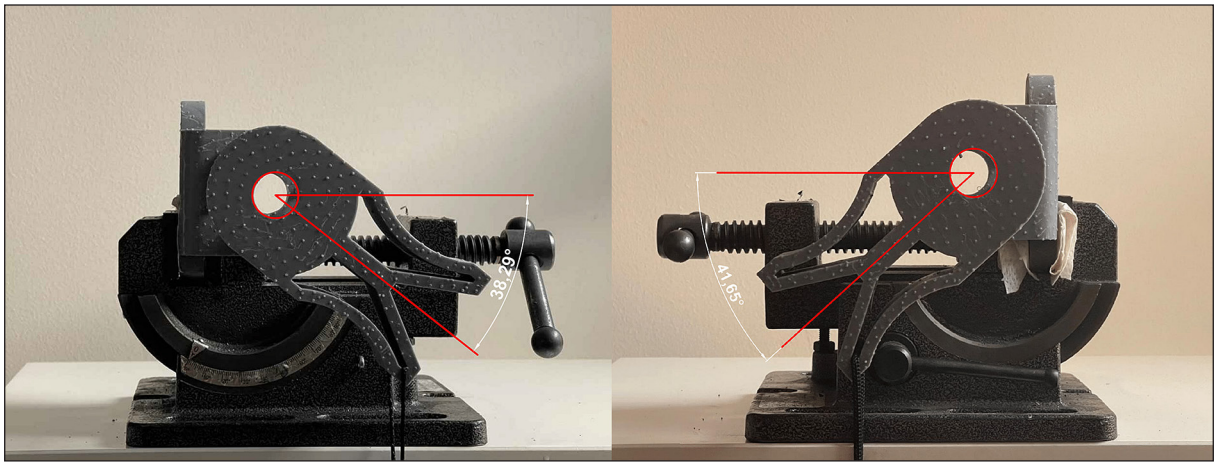

Fig. 27. The maximum obtained rotation angle for the finger with angled beams and the finger with twisted beams

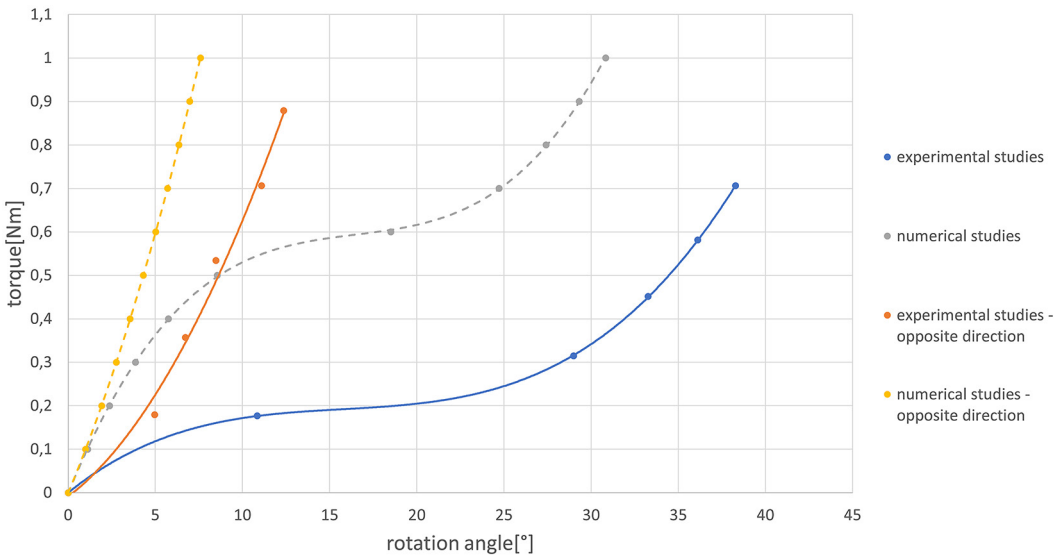

Fig. 28. Comparison of numerical and experimental studies for the model with angled beams

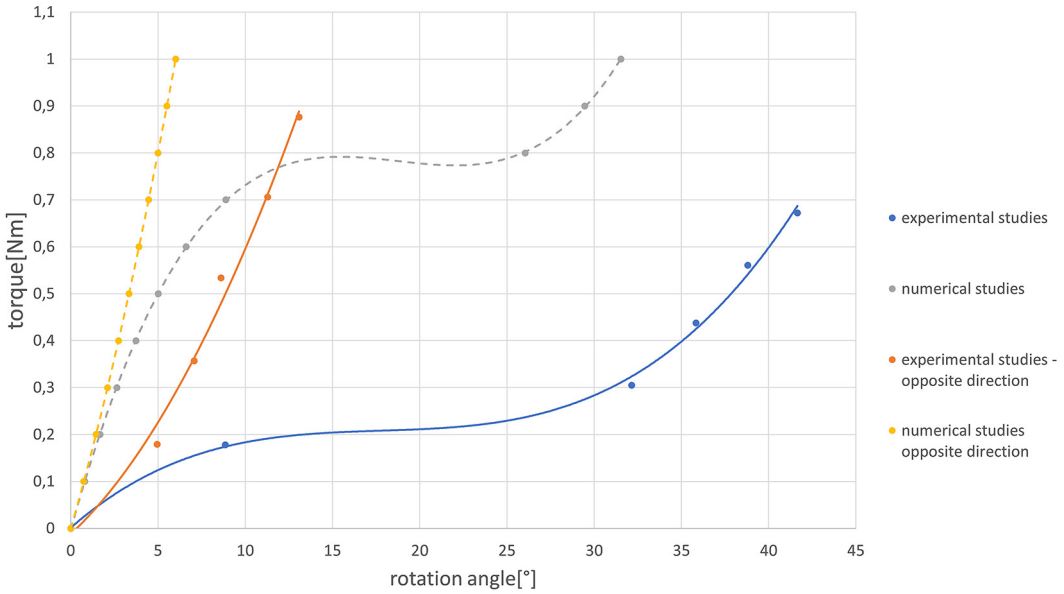

Fig. 29. Comparison of numerical and experimental studies for the model with twisted beams

Table 6. The measurements for the finger with angled beams

Load [kg]	Torque [Nm]	Rotation angle [°]	Torque opposite [Nm]	Rotation angle opposite [°]
0.2	0.18	10.84	0.18	4.96
0.4	0.31	28.99	0.36	6.72
0.6	0.45	33.27	0.53	8.48
0.8	0.58	36.12	0.71	11.10
1	0.71	38.29	0.88	12.36

Table 7. The measurements for the finger with twisted beams

Load [kg]	Torque [Nm]	Rotation angle [°]	Torque opposite [Nm]	Rotation angle opposite [°]
0.2	0.18	8.86	0.18	4.96
0.4	0.30	32.14	0.36	7.07
0.6	0.44	35.84	0.53	8.61
0.8	0.56	38.80	0.71	11.28
1	0.67	41.65	0.88	13.08

are also present. The angle measurement applied may be imprecise, as bending moments acting on the fingers also induce deformations. Differences also arise from assuming linear properties for the material. During the experiment, there might have been an exceeding of the yield point, leading to greater deformations.

CONCLUSIONS

Changing a single characteristic dimension for both revolute joint models leads to radical differences in their torsion characteristics and, consequently, in the stiffness of the models. By altering just one parameter, it is possible to tailor the characteristic curve to specific requirements over a wide range, depending on the needed stiffness for a particular application or the expected rotation angle. Furthermore, local instability of beams can be harnessed to achieve greater rotation angles or very low stiffness values within a certain range of motion. Both models exhibit varying torsional stiffness depending on the direction of the applied moment. The advantage of the twisted beam model is its lower stiffness during instability. By employing these kinematic pairs in gripper fingers, they inherit these benefits. Changing the

geometric parameters of the kinematic pairs alters the torsional stiffness of the fingers as well as their maximum rotation angle.

These fingers offer numerous advantages. They are highly cost-effective to manufacture, and their stiffness characteristics can be easily adjusted. Furthermore, these fingers can facilitate the control of a pneumatic gripper due to their compliance. The force on the fingers increases in accordance with the stiffness characteristic, eliminating the need to be concerned about a sudden force increase during gripping. These fingers also exhibit different stiffness characteristics depending on the gripping side. The finger assembly is universal, allowing for swapping and adjustment to the width of the lifted object. Additionally, it is possible to tailor the geometric parameter values to accommodate the size of the handled object and the gripper's stroke.

The experimental results do not perfectly match the computational results. However, they confirm the torsion characteristic trends of the tested models. The loss of stability and subsequent recovery of stiffness are evident. Additionally, the differing behavior of the kinematic pairs depending on the direction of the moment has been confirmed.

REFERENCES

1. Howell L.L. Compliant Mechanisms. In: McCarthy J., Editors. 21st Century Kinematics. Springer, London, 2013, 189–216.
2. Liu T., Hao G. Design of deployable structures by using bistable compliant mechanisms. Micromachines 2022; 13(5): 651.
3. Carollo G., Ingrassia T., Pantano A. Design of a low cost 3D printable single-component compliant mechanism for FWMAV's wing actuation. In: Proc. of the Second International Conference on Design Tools and Methods in Industrial Engineering, Rome, Italy 2021: 39–49.
4. Ames D.C., Smith G.L., Nathan L., Howell L.L., Magleby S.P. Laser forming of compliant mechanisms. ASME Open Journal of Engineering 2023 January; 2.
5. Stankiewicz G., Dev C., Steinmann P. Geometrically nonlinear design of compliant mechanisms: Topology and shape optimization with stress and curvature constraints. Computer Methods in Applied Mechanics and Engineering 2022 July 1; 397: 115161.
6. Hargrove B., Nastevska A., Frecker M., Jovanova J. Pseudo rigid body model for a nonlinear folding compliant mechanism. Mechanism and Machine Theory 2022 October; 176: 105017.
7. Zolfagharian A., Mohammad L., Ranjbar S., Tadesse Y., Bodaghi M. 3D printing non-assembly compliant joints for soft robotics. Results in Engineering 2022 September; 15: 100558.
8. Xiu H., Han Y., Wang X., Zhang Y., Liang W., Wei G., et al. Design, development, and clinical validation of a two degrees of freedom compliant ankle-foot prosthesis based on a 4-4r parallel mechanism. Mechanism and Machine Theory 2022 June; 172: 104818.
9. Stojiljković D., Milošević M., Ristić-Durrant D., Nikolić V., Pavlović N.T., Ćirić I., et al. Simulation, analysis, and experimentation of the compliant finger as a part of hand-compliant mechanism development. Applied Sciences 2023; 13(4): 2490.
10. Ma W., Liu X., Qiu X., Zhou Y., Liu Y., Fu W., et al. Comparative folding/unfolding performance of notch-type compliant joints. Case Studies in Construction Materials 2023 July; 18: e01760.
11. Chen K., Lai T., Yang F., Zhang J., Yao L. A one-DOF compliant gripper mechanism with four identical twofold-symmetric Bricard linkages. Robotica 2023; 41(4): 1098–1114.
12. Zhang Q., Liu P., Yan P. Design and test of a curved-beam based compliant gripper for manipulations of actively deformable objects. IEEE Access 2022; 10: 102701–102709.
13. Fu J., Lin H., Prathyush I.V.S., Huang X., Zheng L., Gan D. A novel discrete variable stiffness gripper based on the fin ray effect. In: Proc. of the 15th International Conference on Intelligent Robotics and Applications, Harbin, China 2022, 791–802.
14. Teeple C.B., Werfel J., Wood R.J. Multi-dimensional compliance of soft grippers enables gentle interaction with thin, flexible objects. In: Proc. of the 2022 International Conference on Robotics and Automation (ICRA), Philadelphia, PA, USA 2022, 728–734.
15. Szczesiak R., Kowalik M., Cader M. Parametryczny model numeryczny do predykcji właściwości mechanicznych struktur wytwarzanych w technologii FDM z materiałów polimerowych, Polimery, 2018, 63(9): 952–958. DOI:10.14314/polimery.2018.9.7
16. Phrozen Aqua 4K 3D printing resin. [Access: 2023 Oct. 11]. https://phrozen3d.com/products/aqua-gray-4k-resin-phrozen#specs.